ELSEVIER

WHOLE PANCREAS TRANSPLANTATION
Clinical

Present Status of Pancreas Transplantation in Japan—Donation Predominantly From Marginal Donors and Modified Surgical Technique: Report of Japan Pancreas Transplantation Registry

M. Ishibashi, T. Ito, A. Sugitani, H. Furukawa, S. Sekiguchi, M. Gotoh, S. Teraoka, Y. Sato, N. Matsuno, S. Kenmochi, H. Uchida, N. Yoshimura, Y. Nakajima, Y. Kuroda, H. Odan, Y. Idezuki, and Y. Kanazawa

ABSTRACT

In Japan, organ donation has been still limited because of the strict donor criteria. The aim of this study was to show the effectiveness of pancreas transplantation (PTx) by analyzing the outcomes even under poor donor conditions. Thirty-six cases of PTx (32 simultaneous pancreas and kidney transplantations [SPK], 4 pancreas after kidney transplantations) performed during the last 8 years were examined especially for donor characteristics. Mean donor age of 41.4 ± 11.9 years was considerably older compared with that in the United States and Europe; donors aged over 40 years comprised 67% of the total. According to the criteria described by Kapur, 29 cases (81%) in our series would be considered marginal. Thus, to increase blood supply into the pancreatic head, the gastroduodenal artery (GDA) was anastomosed using donor artery to common hepatic artery or iliac Y

From the Department of Urology (M.I.), Nara Medical University Hospital, Nara, Japan; Department of Surgery (T.I.), Osaka University Hospital, Osaka, Japan; Department of Surgery and Oncology (A.S.), Kyushu University Hospital, Fukuoka, Japan; First Department of Surgery and Transplantation (H.F.), Hokkaido University Hospital, Sapporo, Japan; Second Department of Surgery (S.S.), Advanced Surgical Science & Technology, Tohoku University Hospital, Sendai, Japan; First Department of Surgery (M.G.), Fukushima Medical University Hospital, Fukushima, Japan; Third department of Surgery (S.T.), Tokyo Women's Medical University Hospital, Tokyo, Japan; First Department of Surgery (Y.S.), Niigata University Hospital, Niigata, Japan; Department of Surgery (N.M.), Tokyo Medical University-Hachioji Hospital, Tokyo, Japan; Department of Surgery (S.K.), National Chiba-Higashi Hospital, Japan; Department of Transplantation Surgery (H.U.), Nagoya Daini-Red Cross Hospital, Japan; Department of Transplantation and Regenerative Surgery (N.Y.), Kyoto Prefectural University Hospital, Kyoto, Japan; First Department of Surgery (Y.N.), Nara Medical University Hospital, Nara, Japan; Department of Surgery (Y.K.), Kobe University Hospital, Kobe, Japan; Department of Surgery (H.O.), Hiroshma University Hospital, Hiroshima, Japan; Minami-senjyu Hospital (Y.I.), Japan; and Japan Diabetes Foundation (Y.K.), Japan.

Address reprint requests to Michio Ishibashi, Department of Urology, Nara Medical University, 840 Shijo-cho, Kashihara, Nara 634-8522, Japan. E-mail: imichio@nmu-gw.naramed-u.ac.jp

0041-1345/08/$–see front matter
doi:10.1016/j.transproceed.2008.01.047

graft. These procedures were performed in 16 of the 24 cases in which there was liver procurement. Eventually, 34 cases (94%) preserved GDA continuity. Mean total cold ischemic time of pancreatic grafts was 12 hours 15 minutes. Of 214 registrants, 17 patients on the waiting list for SPK died of diabetic complications. To date, patient survival remains 100% with a mean follow-up period of 33 months. Pancreas graft survivals at 1, 3, and 5 years posttransplantation were 92%, 80%, and 80%, respectively. In contrast, kidney survivals were 91%, 91%, and 91%, respectively. The integrity of the pancreas head and duodenum by preservation of the GDA continuity might have decreased the risk associated with the marginal donors.

SIMULTANEOUS PANCREAS and kidney transplantation (SPK) is an established treatment for type I diabetes with end-stage renal disease. The recent reports describe 85% pancreas graft survival rate at 1 year and 92% kidney graft survival.[1,2] However, the surgical complications continue to relate to pancreatic duct management of enteric drainage (ED) or ischemic reperfusion injury.[1]

The Organ Transplant Law was enforced in Japan on October 1997. Since 2000, 44 pancreas transplantation (PTx) cases have been derived from 34 brain-dead donors, two non-heart-beating donors (NHBDs), and eight living donors. In our country, organ donation is still limited due to strict donor criteria. Further, most donors are considered marginal because of their poor condition. The aim of this study was to show the effectiveness of PTx outcomes even under poor donor conditions.

PATIENTS AND METHODS

Patients and Indication for PTx

From November 1999 to the end of April 2007, the Japan Organ Transplantation Network (JOTNW) registered 214 patients for PTx. The indication for PTx for type I diabetic patients was similar to that of the American Association of Diabetes,[3] except that a state of absolute deficiency of insulin secretion with less than 0.5 ng/mL serum C-peptide was mandatory. Out of 214 registrants, 181 patients were listed for SPK, 25 patients for pancreas after kidney transplantation (PAK), and the remaining eight patients for pancreas transplantation alone.

Current Organization of PTx Program and 14 Hospitals for PTx

To achieve the satisfactory result, a "Central Regulation Board" composed of three Japanese medical associations—the Japan Societies for Diabetology, Nephrology and Transplantation—was established in 1997, under the following two policies: one was to participate in an Expert Medical Board of two diabetologists and two nephrologists, located in seven regions of Japan, whose mission was to evaluate PTx candidates. Another policy was the participation in an Expert Surgeon Board, composed of three to seven experienced surgeons.[4,5]

Currently, 14 PTx hospitals approved by the "Central Regulation Board" were authorized by the Organ Transplantation Committee of the Ministry of Health and Welfare.

Allocation Criteria

Kidney and pancreas allocation criteria in Japan were considered to be: one donor kidney shared with at least one HLA-DR antigen preferentially allocated to recipients for SPK.[4,5]

Criteria of Marginal Donor

The criteria of a marginal donor for PTx of Kapur et al were used: donors over 45 years of age, hemodynamically unstable donors at the time of harvest (with dopamine dose > 10 μg/k/min, or two or more vasopressors), or an NHBD.[6] Our indications for NHBD were described previously: age less than 40 years old and the cessation of respirator support allowed by the family of the deceased person.[4,5]

Gastroduodenal Artery Reconstruction

In cases of simultaneous liver and pancreas procurement, the hepatic artery (HA) was given priority to the liver team. The procedure of gastroduodenal artery (GDA) reconstruction varied based on the dissection site of the HA of the liver graft. When the stump of the proper HA with the GDA was preserved, direct suture of the stump of proper HA was done, designated as pattern I. In cases of preservation of the splenic artery with the stump of common hepatic artery (CHA), a donor iliac artery was interposed between stump of CHA and GDA, designated as pattern II.[4,5] When CHA was removed with the celiac trunk, various choices for reconstruction using donor iliac graft artery were performed (pattern III). One example showed that the donor iliac artery graft extended to the GDA was anastomosed to end-to-side of the Y-graft (Fig 1).[5]

Graft Survival Rate

Thirty-six cases were observed from April 2000 to the end of April 2007. Pancreas grafts were considered functioning as long as the recipients were insulin independent, and death with a functioning graft was considered be a graft failure.[1] Graft survival rates were calculated by the Kaplan-Meier procedure.

RESULTS

Numbers of PTx

During the last 8 years, we performed 48 cases of multiple organ transplantation, such as heart, lung, liver, pancreas, kidney, and small intestine, from heart-beating donors. The 48 cases included 34 PTx with 14 organs not transplanted because of medical reasons (n = 7), and the remaining seven cases were not allocated by the allocation criteria.

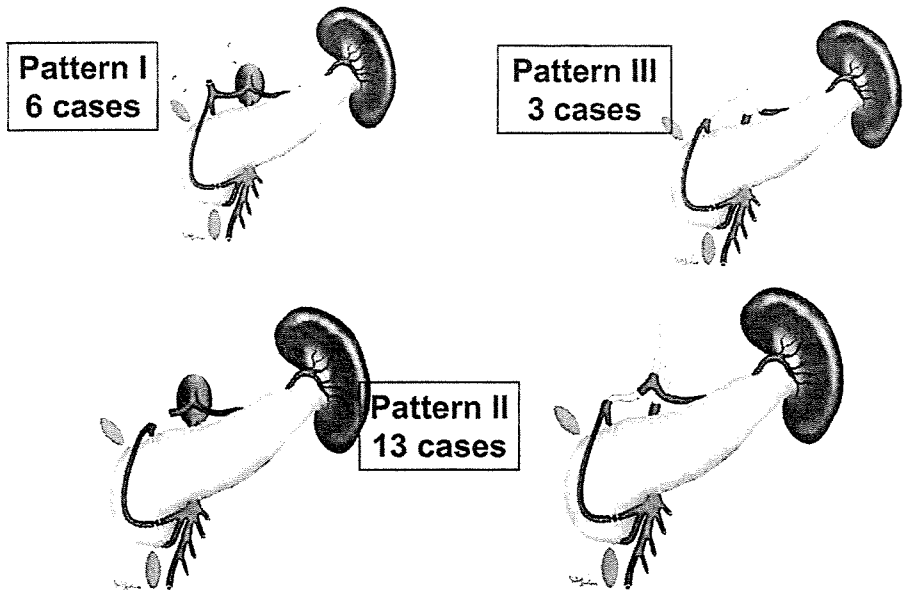

Fig 1. Frequency of three pattern of GDA reconstruction in 22 pancreas grafts.

Two cases of PTx from NHBDs were done. Among the 36 PTx cases, 32 received SPK and four PAK. Finally, 36 cases of 214 registrants received PTx, 17 cases listed for SPK were dead, eight cases were canceled for registrants, and 153 cases continue to wait for PTx.

Characteristics of 36 Pancreas Donors

The mean donor age was 41.4 ± 11.9 years old. Male donors accounted for 42%. The mean body mass index was 22% ± 4%. Twenty-nine cases (81%) were categorized as marginal donors. The main cause of death was due to nontrauma: six for trauma, 22 for cerebrovascular accident, seven for post–cardiopulmonary resuscitation, and one for brain tumor. Twenty-four (67%) cases donated both liver and pancreas.

Table 1 shows the age distribution of the 36 cases. Among the donors less than 40 years old, 33% were considered marginal, indicating hemodynamically unstable cases. Therefore, the 36 pancreas donors demonstrated a high percentage of marginal donors.

Table 1. Age Distribution of 36 Pancreas Donors

Age (y)	Number of donors (n = 36)	Number of marginal cases (n = 29)
<18	0	0
18–40	15 (42%)	12 (33%)
41–50	11 (31%)	7 (19%)
51–55	4 (11%)	4 (11%)
56–60	6 (17%)	6 (17%)
Mean of age	41.4 ± 11.9	42.2 ± 12.8

Pattern of GDA Reconstruction

To increase blood flow in the graft pancreas head and duodenum, we performed reconstruction of the GDA as often as possible. According to Donatini, anterior-superior pancreaticoduodenal artery arising from GDA is the main artery to the pancreas head, especially to the anterior part of pancreas head, which less frequently communicated with anterior-inferior pancreaticoduodenal artery.[7] GDA was reconstructed according to the dissection site, as shown in Fig 1. Pattern II was most frequent. Of 36 PTx, 34 cases preserved the GDA continuity by either vascular reconstruction in 22 cases or nondissected GDA in 12 cases. Only in two cases was GDA ligated. Donor iliac graft artery was principally used, although unequal size mismatch of artery was common. Only one case reconstructed by graft mesenteric artery lost the pancreas graft due to uncontrollable perforation of graft duodenum at 1 year after PTx.

Patient and Graft Survivals

All patients were alive throughout the observation. One-, 3-, and 5-year pancreas and kidney graft survivals were 91.7% and 90.6%, 80.2% and 90.6%, and 80.2% and 90.6%, respectively, which were equivalent to those in the United States and Europe.[1,2]

With respect to the effect of marginal donors on pancreas graft survival, 1- and 3-year graft survivals of 29 cases transplanted from marginal donors were 90% and 76%, in contrast to the seven cases from nonmarginal donor of 100%. Concerning kidney graft survival rates, the similar tendency was observed: 3-year graft survival rate of 27 marginal cases was 74%, while that of five nonmarginal cases was 100%.

Currently, 30 pancreas transplant patients are off insulin; one case prescribed oral hypoglycemic agents is still considered insulin independent.

Demographics of 36 Pancreas Recipients

Table 2 shows the demographics of 36 pancreas recipients. Age, gender, duration of diabetes, duration of dialysis therapy, number of mismatched HLA-A,B,DR antigens were not remarkable. The mean total cold ischemic time was 726 minutes. Tacrolimus/cyclosporine plus mycophenolate mofetil and prednisolone with antibody induction mainly by anti-interleukin-2 receptor monoclonal antibody was more frequently used. Concerning duct management, ED was more frequently adopted than bladder drainage, because of fewer complications.

Surgical Complications

Table 3 shows only surgical complications, in which nine cases (25%) needed relaparotomy within 1 year after PTx. No leakage or bleeding of the graft duodenum anastomotic site was observed; there was one case of fluid collection due to graft pancreatitis. All patients with the complications were alive. In the late phase of 1 year after PTx, one case of graft loss was due to duodenal perforation.

Cause of Pancreas Graft Loss

Five pancreas grafts were lost during the observation. Two cases of venous thrombosis occurred on days 6 and 9 after SPK. One arterial thrombosis on day 2 was observed. At 1 year after SPK, one pancreas graft with a duodenal perforation was lost. One chronic rejection case became insulin dependent after 3 years.

Delayed Graft Function

The incidence of delayed pancreas graft function, requiring exogenous insulin administration for more than 4 weeks post-PTx, was observed in 14 cases (38%). The incidence of delayed kidney graft function, requiring hemodialysis postoperatively, was eight cases (22%); one case was lost due to primary nonfunction.

Table 2. Demographics of 36 Pancreas Recipients

Age, y (median)	37 (29–54)
Gender (male/female)	18/18
Duration of IDDM (y)	24 (9–34)
Duration of dialysis (y)	4.6 (1–6)
Waiting time (d)	944 ± 652
Total cold ischemic time (min)	726 ± 174
Ratio of marginal donor	29/36 (81%)
Number of mismatched HLA-A,B,DR	2.7 ± 1.1
Immunosuppressive regimens	
FK/CyA-MMF-P with antibody	33
FK/CyA-MMF-P without antibody	3
Duct management (BD/ED)	10/26
GDA continuity (yes/no)	34/2
Arterial reconstruction	24
Nondissected, preserved GDA	12

Table 3. Cause and Onset of Surgical Complications Requiring Relaporotomy

Cause of Relaparotomy	< 1 year	> 1 year
Venous thrombosis	2	
Arterial thrombosis	1	
Bleeding of graft, not anastomotic	2	
Wound dehiscence	1	
Fluid collection	1	
Conversion to ED	2	2
Perforation of graft duodenum		1
Bleeding of graft duodenum after ED conversion at 18 mo of post-TX		1
Hernia in abdominal wall		3
Totals	9/36 (25%)	7/36 (19%)

DISCUSSION

Our major concern in facing the beginning of PTx was how to achieve an 80% pancreas graft survival rate at 1 year due to the difficult conditions around pancreas transplantation, such as the low number of donations and higher incidence of marginal cases. One solution was to organize as collaboration of PTx including not only pancreas transplant surgeons, but also physicians, diabetologists, and nephrologists.

Another solution was to introduce aggressive surgical procedures to preserve GDA continuity (Fig 1). Pattern II was available frequently, since liver transplant surgeons in our country do not need to remove the celiac trunk, because they had much experience with living related liver transplantation. In fact, in our initial case of pancreas transplant from a marginal case, the liver surgeon gave us a good opportunity to reconstruct the GDA continuity by placement of an interposed graft iliac artery between the stump of GDA and that of the CHA. Thus, those difficulties with pancreas donation led us to choose a modified surgical technique.

Compared with the conditions of pancreas donors in the United States and Europe,[1,2] most cases of PTx used organs from marginal donors. We less frequently noticed graft pancreatitis or bleeding or leakage of the anastomatic site of duct management. Increasing blood flow to the pancreas head and duodenum of transplant from marginal donors might decrease ischemic-reperfusion injury. As the importance of pancreas head and duodenum integrity has been suggested,[4,5,8,9] we await validation of preserving GDA continuity by the modified surgical technique.

ACKNOWLEDGMENT

We acknowledge Prof K. Nomoto, Mrs Kawamura, and Mrs Mikami of JOTNW, and Mrs Y. Saito of Japan Diabetes Foundation for the preparation of Japan Pancreas Transplant Registry Report.

REFERENCES

1. Gruessner AC, Sutherland DER: Pancreas transplant outcomes for United States (US) and non-US cases as reported to the United Network for Organ Sharing (UNOS) and International Pancreas Transplant Registry (IPTR) as of June 2004. Clin Transplant 19:433, 2005

2. Andreoni KA, Brayman KL, Guidinger MK, et al: Kidney and pancreas transplantation in the United States, 1996–2005. Am J Transplant 7(Part 2):1359, 2007

3. American Diabetes Association: Pancreas and islet transplantation in type 1 diabetes. Diabetes Care 29:935, 2006

4. Ishibashi M, Ito T, Sugitani A, et al: Characteristics of pancreas transplantation currently performed in Japan. Transplant Proc 36:1086, 2004

5. Ito T, Ishibashi M, Sugitani A, et al: Present status of pancreas transplantation in Japan. In: Cecka JM, Terasaki PI (eds): Clinical Transplants 2004. Los Angeles, Calif: UCLA Immunogenetics Center; 2004, p 167

6. Kapur S, Bonham CA, Dodson SF, et al: Strategies to expand the donor pool for pancreas transplantation. Transplantation 67: 284, 1999

7. Donatini B: A systematic study of the vascularization of the pancreas. Surg Radiol Anat 12:173, 1990

8. Nghiem DD: Role of bench angiography in the assessment of pancreaticoduodenal graft blood supply. Transplant Proc 30:256, 1998

9. Socci C, Orsenigo E, Zuber V, et al: Triple arterial reconstruction improves vascularization of whole pancreas for transplantation. Transplant Proc 38:1158, 2006

ELSEVIER

Two Cases of Calcineurin Inhibitor-Associated Reversible Posterior Leukoencephalopathy Syndrome in Renal Transplant Recipients

N. Akutsu, C. Iwashita, M. Maruyama, K. Ootsuki, T. Ito, K. Saigo, and T. Kenmochi

ABSTRACT

Reversible posterior leukoencephalopathy syndrome (RPLS) is one of the important side effects of calcineurin inhibitors (CNIs). Magnetic resonance imaging (MRI) of the brain is useful for the diagnosis of RPLS, showing the edema primarily in the cortex and subcortical white matter of the posterior brain regions. Interruption of CNIs is essential for the treatment of patients with RPLS. Herein we have described 2 cases (1.7%) of RPLS induced by CNIs after kidney transplantation. The first case was a 56-year-old man with chronic renal failure due to diabetic nephropathy who received a living-related kidney transplantation in 2006. Initial immunosuppressive therapy consisted of cyclosporine, mycophenolate mofetil (MMF), prednisolone, and basiliximab. Four months after transplantation, he developed unconsciousness and paralysis. The second case was a 24-year-old woman with end-stage renal disease due to Alport syndrome who received an ABO-incompatible living-related kidney transplantation. Initial immunosuppressive therapy consisted of tacrolimus, MMF, prednisolone, and basiliximab. On postoperative day 3, she developed convulsions and unconsciousness. In both patients, RPLS was diagnosed with neurological symptoms and MRI findings at early stage of the disease, and they recovered rapidly from the disease by the interruption of CNIs. Our data demonstrated that early diagnosis and immediate interruption of CNIs were essential for the treatment of RPLS after kidney transplantation.

CALCINEURIN INHIBITORS (CNIs)—cyclosporine (CsA) and tacrolimus—are potent immunosuppressive agents widely used in organ transplantation of the kidney. However, neurological complications of CNIs such as convulsions, headache, and unconsciousness have been reported frequently in addition to multiple other organ toxicities.[1] Neurotoxicity of these agents for the central nervous system has been increasingly reported with the widespread use of magnetic resonance imaging (MRI). Reversible posterior leukoencephalopathy syndrome (RPLS) occurs in patients with acute hypertension caused by various conditions or those who are immunosuppressed. In patients with RPLS, MRI of the brain shows edema primarily in the cortex and subcortical white matter of the posterior brain regions, such as the occipital lobes and posterior parietal lobes. The brain edema is generally reversible, disappearing upon normalization of blood pressure and interruption of immunosuppressive agents.[2,3] With the recent widespread use of MRI, this complex syndrome has become more familiar. Herein we have described 2 cases of RPLS induced by CNIs after kidney transplantation.

CASE REPORTS

Case 1

The first case, a 56-year-old man with chronic renal failure due to diabetic nephropathy, received an ABO-matched living-related donor kidney transplant in 2006. The donor was his 52-year-old brother. Initial immunosuppressive therapy consisted of CsA, mycophenolate mofetil (MMF), prednisolone, and basiliximab. Four months after transplantation, he was admitted with pneumocystis pneumonia, receiving treatment with pentamidine and sulfamethoxazole-trimethoprim. During the hospitalization, he developed unconsciousness and paralysis. MRI of the brain clearly

From the Department of Surgery, Chiba-East Hospital, National Hospital Organization, Chiba, Japan.

This work was supported by a Grant-in-Aid for Scientific Research (C) (18591426) of Japan Society for the Promotion of Science (JSPS).

Address reprint requests to Naotake Akutsu, Department of Surgery, Chiba-East Hospital, National Hospital Organization, 673 Nitona, Chuo-ku, Chiba-City, Chiba 260-8712, Japan. E-mail: nakutsu@nitona.hosp.go.jp

0041-1345/08/$-see front matter
doi:10.1016/j.transproceed.2008.07.104

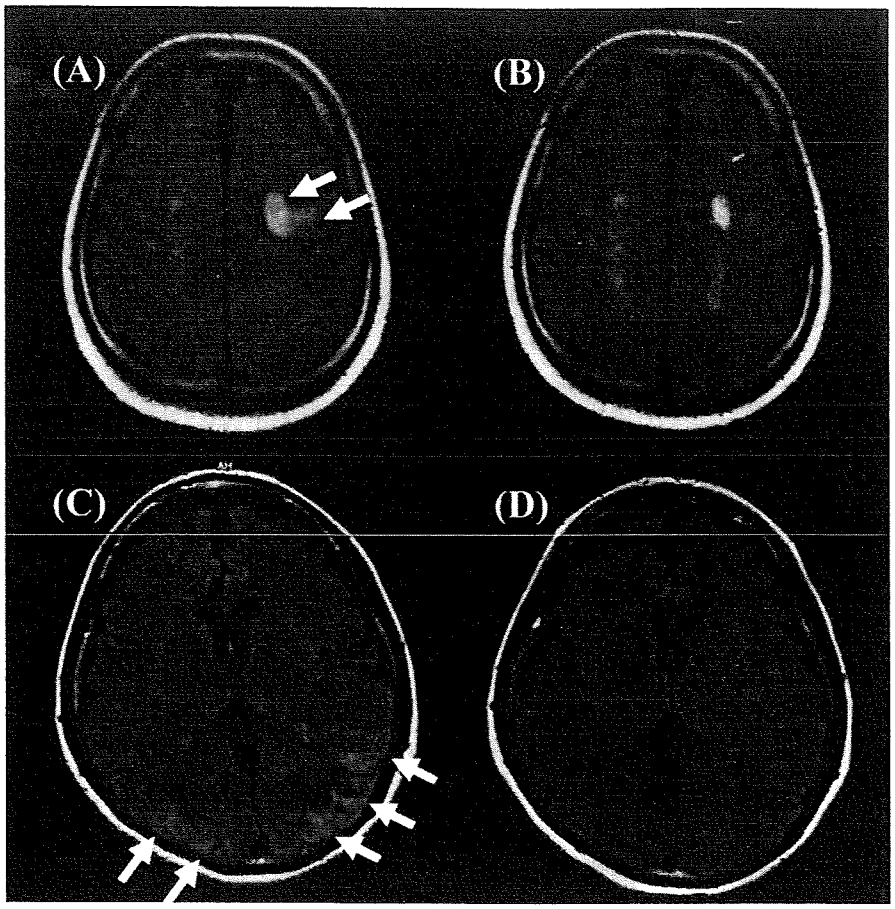

Fig 1. Axial MRI FLAIR images of RPLS case 1 **(A,B)** and case 2 **(C,D)**. In case 1, high signal intensity patchy areas (arrows) are indicated in the right temporoparietal region at 4 months after transplantation (A). In the same FLAIR image (B) obtained 2 months after CsA therapy interruption, a subtotal disappearance of the signal intensity abnormalities of RPLS is noted. In case 2, high signal intensity patchy areas (arrows) are indicated in the posterior regions at 3 days after transplantation (C). In the same FLAIR image (D) obtained 2 weeks after tacrolimus therapy interruption, a complete disappearance of the signal intensity abnormalities of RPLS is noted.

demonstrated multiple bilateral focal areas of hyperintensity in both T2-weighted and FLAIR images, predominantly in the cortical white matter and partially in the subcortical matter (Fig 1A). We diagnosed him as RPLS due to CsA neurotoxicity, since the blood trough concentration of CsA was elevated to 778 ng/mL. Serum magnesium and cholesterol levels were within the normal ranges. CsA was converted to tacrolimus; the symptoms rapidly and completely disappeared. Also, MRI abnormalities gradually improved and he was discharged 3 months after the onset of RPLS.

Case 2

The second case, a 24-year-old woman with end-stage renal disease due to Alport syndrome, received an ABO-incompatible living-related kidney transplant in 2007. The donor was her 51-year-old mother. Kidney transplantation was performed preemptively before undergoing hemodialysis. A splenectomy was followed by the kidney transplantation. Initial immunosuppressive therapy consisted of tacrolimus, prednisolone, MMF, and basiliximab. Three days after transplantation, she suddenly developed convulsions. Similar to case 1, initial cranial MRI revealed multiple bilateral focal hyperintensity areas in FLAIR images, predominantly in the white and gray matter of the occipital and posterior parietal lobes (Fig 1C). The cause of her RPLS was considered to be tacrolimus neurotoxicity since its trough level was elevated to 56 ng/mL. Following reduction of tacrolimus, both clinical symptoms and the abnormal shadows in MRI quickly disappeared. She was discharged at 2 months after kidney transplantation.

DISCUSSION

Acute neurological side effects produced by CNIs have been widely described. The frequency of CsA-induced neurotoxicity has been reported to range from 25% to 35%.[4] Also, the frequency of tacrolimus neurotoxicity has been observed among 32% of cases.[5] Recently, RPLS has been increasingly reported with the widespread use of MRI. From April 2004 to November 2007, we performed 117 kidney transplantations, experiencing 2 cases (1.7%) of CNI-induced RPLS. In both patients, CNI trough levels were elevated to toxic levels. At early stages of the disease, RPLS was diagnosed by neurological symptoms and MRI findings. After interruption of CNIs, both patients recovered rapidly without neurological deficits. RPLS in the cases may have occurred due to other immunosuppressive drugs, such as MMF, prednisolone, and basiliximab.[6] Neurotoxicity has been reported with MMF; however, withdrawal of RPLS symptoms after interruption of CNIs suggested that they caused RPLS in our cases.

We have a lot of questions to resolve the exact mechanisms of RPLS. Hypertension, vascular injury, endothelin, hypomagnesemia, hypocholesterolemia, and thrombotic microangiopathy are thought to be related to CNI-associated RPLS.[1] In our first case, hypertension and elevated trough levels of CsA were considered to be the major causes of RPLS. In addition, the patient had severe diabetes mellitus, which may stimulate CsA toxicity on the central nerve system. In the second case, a high trough level of tacrolimus was detected at the onset of PRLS. Although it was not clear why the trough level of tacrolimus was elevated, this case suggests the need to monitor blood concentrations frequently in the early days after transplantation.

For the early diagnosis of RPLS, MRI is the most potent tool, usually revealing abnormal shadows, including both gray and white matter, which are diffuse but predominantly involve 4 major regions of the cerebral hemispheres: occipital poles; parietal poles; frontoparietal junction; and inferior temporo-occipital junction. This pattern corresponds to the watershed zones between the main branches of the cerebral arteries.[7] Treatment with antihypertensive agents or reduction or withdrawal of CNIs has been reported to lead to resolution of neurological signs and neuroimaging abnormalities within weeks in all patients.[8] However, it has been reported that this syndrome may result in an irreversible neurological deficit.[9,10] In this report, 2 patients manifested characteristic radiological findings on initial MRI. These changes almost completely resolved on follow-up MRI after withdrawal of the causative CNI. In the first case, clinical symptoms but not MRI findings completely disappeared after cessation of CsA, suggesting that early diagnosis and treatment are important. In general, the prognosis of CNI neurotoxicity is good. Even severe complications, such as RPLS, are resolved with drug dose reduction or withdrawal.[11]

Recently, MMF and daclizumab have received attention as substitutable drugs for CNIs; several trials are ongoing with regimens using these agents, which permit reduction or elimination of CNIs and associated toxicities, particularly neurotoxicity and nephrotoxicity. Since a high frequency of acute rejection has been reported among patients on treatment without CNIs, at least a low dose CNIs is still believed to be necessary in primary renal transplant immunosuppression.[12] In our cases, it was possible that elimination of CNIs would lead to allograft rejection. Therefore, we converted them using an alternate CNIs; the grafts survived and functioned. Immunosuppressive regimens with better renal function and less toxicity are expected to improve long-term allograft survival.

In conclusion, we demonstrated that RPLS as the neurotoxicity of CNIs was reversible in both clinical symptoms and MRI findings. In cases of unconsciousness or convulsions after organ transplantations, RPLS should be considered. Early diagnosis using MRI with immediate interruption or conversion of CNIs is essential to cure RPLS without a neurological deficit.

REFERENCES

1. Gijtenbeek JMM, van den Bent MJ, Vecht ChJ: Cyclosporine neurotoxicity: a review. J Neurol 246:339, 1999
2. Munoz R, Espinoza O, Espinoza A, et al: Cyclosporine-associated leukoencephalopathy in organ transplant recipients: experience of three clinical cases. Transplant Proc 38:921, 2006
3. Kwon S, Koo J, Lee S: Clinical spectrum of reversible posterior leukoencephalopathy syndrome. Pediatr Neurol 24:361, 2001
4. Truwit CL, Denaro CP, Lake JR, et al: MR imaging of reversible cyclosporine A-induced neurotoxicity. Am J Neuroradiol 12:651, 1991
5. Widjdicks EFM, Wiesnwe RH, Dahlke LJ, et al: FK-506-induced neurotoxicity in liver transplantation. Ann Neurol 35:498, 1994
6. Barshes NR, Goodpastor SE, Goss JA: Pharmacologic immunosuppression. Front Biosci 9:411, 2004
7. Bartynski W, Zeigler Z, Spearman P, et al: Etiology of cortical and white matter lesions in cyclosporin-A and FK-506 neurotoxicity. Am J Neuroradiol 22:1901, 2001
8. Hinchey J, Chaves C, Appignani B, et al: A reversible posterior leukoencephalopathy syndrome. N Engl J Med 334:494, 1996
9. Antunes NL, Small TN, George D, et al: Posterior leukoencephalopathy syndrome may not be reversible. Pediatr Neurol 20:241, 1999
10. Cooney MJ, Bradley WG, Symko SC, et al: Hypertensive encephalopathy: complication in children treated for myeloproliferative disorders—report of three cases. Radiology 214:711, 2000
11. Belli LS, De Carlis L, Romani F, et al: Dysarthria and cerebellar ataxia: late occurrence of severe neurotoxicity in a liver transplant recipient. Transpl Int 6:176, 1993
12. Ekberg H, Tedesco-Silva H, Demirbas A, et al: Reduced exposure to calcineurin inhibitors in renal transplantation. N Engl J Med 357:2562, 2007

HUMAN MUTATION 29(5), 703–708, 2008

RESEARCH ARTICLE

Integration of Hepatitis B Virus DNA Into the Myeloid/Lymphoid or Mixed-Lineage Leukemia (*MLL4*) Gene and Rearrangements of *MLL4* in Human Hepatocellular Carcinoma

Kenichi Saigo,[1,2] Kenichi Yoshida,[3]* Ryuji Ikeda,[3] Yoshiko Sakamoto,[3] Yoshiki Murakami,[4] Tetsuro Urashima,[1] Takehide Asano,[5] Takashi Kenmochi,[2] and Ituro Inoue[3,6]

[1]*Second Department of Surgery, School of Medicine, Chiba University, Chiba, Japan;* [2]*Clinical Research Center, Chiba-East National Hospital, Chiba, Japan;* [3]*Division of Genetic Diagnosis, Institute of Medical Science, University of Tokyo, Tokyo, Japan;* [4]*Center for Genomic Medicine, Kyoto University Graduate School of Medicine, Kyoto, Japan;* [5]*Hepato-Pancreato-Biliary Surgery, School of Medicine, Teikyo University, Tokyo, Japan;* [6]*Division of Molecular Life Science, School of Medicine, Tokai University, Kanagawa, Japan*

Communicated by Dr. Haig H. Kazazian, Jr.

Integration of hepatitis B virus (HBV) DNA into host DNA is detected in about 90% of HBV-related hepatocellular carcinoma (HCC), but the preferential sites of the viral integration etiologically relevant to oncogenesis have been controversial. By using an adaptor-ligation/suppression-PCR, we identified four integrations into the myeloid/lymphoid or mixed-lineage leukemia 4 (*MLL4*) gene from 10 HCC patients with positive HBV surface antigen (HBsAg). Determination of the cellular-virus DNA junction demonstrated that various lengths of the virus were integrated within 300 bp of intron 3 flanked by the Alu element of *MLL4*. Chimeric hepatitis B virus X gene (HBx)/*MLL4* transcripts and the HBx fusion proteins were detected. DNA microarray revealed that HBx/MLL4 fusion proteins suppressed unique genes in HepG2 cells. Finally, chromosomal translocations of intron 3 of *MLL4* to the specific region of chromosome 17p11.2 in 22 out of 32 HCC patients were observed, showing that the intron 3 region of *MLL4* gene would be a target of translocation breakpoint. In conclusion, the present data suggest that the translocation breakpoint of *MLL4* gene is one of the preferential targets for HBV DNA integration into the *MLL4* gene and the HBV DNA integration may be involved in liver oncogenesis. Hum Mutat 29(5), 703–708, 2008. © 2008 Wiley-Liss, Inc.

KEY WORDS: hepatocellular carcinoma; DNA integration; hepatitis B virus; HBx; *MLL4*

INTRODUCTION

Chronic human hepatitis B virus (HBV) infection causes mild to severe liver diseases, such as chronic hepatitis, liver cirrhosis, and hepatocellular carcinoma (HCC) [Block et al., 2003]. Nearly 25% of patients with chronic HBV infections terminate in untreatable liver cancer. HBV DNA frequently integrates into the human host genome, whereby insertional mutagenesis plays a crucial role in oncogenesis [Brechot et al., 2000; Gozuacik et al., 2001]. Although integration of HBV DNA is thought to be involved in oncogenesis of human hepatocytes, preferential HBV DNA integration sites targeting cellular genes were not identified until recently. Two groups have reported that HBV DNA is preferentially integrated into the human telomerase reverse transcriptase (*TERT*) gene (MIM# 187270) in HCC [Ferber et al., 2003; Paterlini-Brechot et al., 2003].

In this study, we investigated the integrated HBV DNA and flanking cellular DNA sequences. In four cases, integrations of HBV DNA into intron 3 of the myeloid/lymphoid or mixed-lineage leukemia 4 (*MLL4*) gene (MIM# 606834) were demonstrated, indicating that *MLL4* serves as a cellular target for HBV in liver oncogenesis. The *MLL4* gene is a human member of the *MLL* gene family locating on chromosome 19q13.1 [FitzGerald and Diaz, 1999], where a frequent rearrangement or amplification has been reported in solid tumors [Mitelman et al., 1997; Curtis et al., 1998]. Subsequently, we detected chromosomal translocation between intron 3 of *MLL4* and a specific region of chromosome17p11.2 in 22 HCC samples. These results indicate that intron 3 of the *MLL4* gene is one of the sites of translocation break point, which serves as a preferential target for HBV DNA integration, and may be implicated in the etiology of liver oncogenesis.

The Supplementary Material referred to in this article can be accessed at http://www.interscience.wiley.com/jpages/1059-7794/suppmat.

Received 18 September 2007; accepted revised manuscript 16 November 2007.

*Correspondence to: Kenichi Yoshida, Department of Life Sciences, Meiji University School of Agriculture, 1-1-1 Higashimita, Tama-ku, Kawasaki, Kanagawa 214-8571, Japan (present address). E-mail: yoshida@isc.meiji.ac.jp

Grant sponsor: CREST of Japan Science and Technology (II).
DOI 10.1002/humu.20701
Published online 4 March 2008 in Wiley InterScience (www.interscience.wiley.com).

PATIENTS AND METHODS

Patients

We studied 32 Japanese patients with HCC who had undergone hepatic resection without preoperative therapies at The Second Department of Surgery, Chiba University Hospital between 1987 and 2003. Serological tests for HBV were done by EIA kit (Dainabot, Tokyo, Japan) for HBV surface antigen (HBsAg), and RIA kits (Dainabot) for anti-HBs and anti-HBc antibodies. Anti-HCV antibody was tested by a recombinant immunoblot assay (Ortho Diagnostic, Westwood, MA). The study protocol conformed to the ethical guidelines of the Declaration of Helsinki (1975) and was approved by the Institutional Review Board (IRB) of Chiba University, School of Medicine. All patients gave written informed consent.

PCR and Southern Blot

HBV/cellular DNA junctions in the tumor tissues were analyzed by an adaptor-ligation/suppression-PCR [Siebert et al., 1995], according to Genomewalker Kits (Clonetech, Mountain View, CA) (Supplementary Fig. S1, available online at http://www.interscience.wiley.com/jpages/1059-7794/suppmat). Primer sequences used for PCR detection of HBV/*MLL4* and *MLL4*/HBV junctions and chromosome 19/chromosome 17 boundaries are listed in Supplementary Table S1.

Hind III-digested DNA (10 μg) were electrophoresed on 1.0% agarose gel and blotted onto nylon membrane (Hybond N+; GE Healthcare, Buckinghamshire, UK). The membrane was first hybridized with ^{32}P-labeled hepatitis B virus X gene (HBx) probe and the blot was autoradiographed. After dehybridization of the same membrane, a rehybridization was carried out with ^{32}P-labeled *MLL4* probe (the PCR products spanning exon 4 and exon 5) and autoradiographed.

RT-PCR

Total cellular RNA was extracted using Trizol (Invitrogen, Carlsbad, CA). An RT-PCR was performed with SuperScript One-Step RT-PCR system (Invitrogen) with gene-specific primers on exon 5 and exon 6 of *MLL4*. MD26c primer was used as the common sense primer. The PCR products were subjected to sequencing analyses.

Immunoprecipitation and Western Blot

Tumor tissues were lysed in a buffer containing 0.1% SDS, 0.5% deoxycholate, 1% NP-40, 150 mM NaCl, 50 mM Tris-HCl (pH 8.0), protease inhibitors (complete protease inhibitor tablets; Roche, Basel, Switzerland), and centrifuged. The supernatant was incubated with anti-HBx monoclonal antibody, generously provided by Dr. Yosef Shaul (Weizman Institute of Science), and immunoprecipitation/Western blot was performed with a standard protocol. Anti-Flag antibody was purchased from Sigma-Aldrich (St. Louis, MO).

HBx/*MLL4* Expression Plasmid, Transfection, and DNA Microarray

The HBx expression vector, pECE-X, was a gift of Dr. Jinghsiung James Ou (University of Southern California). Human *MLL4* partial cDNA clone KIAA0304 (accession number AB002302.2) was obtained from Kazusa DNA Research Institute (Chiba, Japan). We deleted intron 7 sequence from KIAA0304 and constructed N-terminally Flag-tagged HBx/*MLL4* chimeric sequence in pcDNA3 (Invitrogen). Human hepatoma cell line HepG2 (RCB1648; RIKEN Cell Bank, Tsukuba, Japan) were transfected using Lipofectamine (Invitrogen). After 48 hr of transfection, total RNA was recovered and the microarray analysis including 12,814 unique clones from Incyte UniGene 1 was performed according to the manufacturer's instructions (Agilent Technologies, Santa Clara, CA).

RESULTS

Detection and Sequence Analysis of HBV/Cellular DNA Junctions

A total of 10 tumor specimens from HCC patients with positive HBsAg were examined for HBV DNA (accession number AB033550.1) integrations into cellular genome. The clinical backgrounds of the patients are summarized (Supplementary Table S2). We could detect four integrations into the *MLL4* gene on chromosome 19q13.1 and one into the *TERT* gene (Table 1). Integration sites of *MLL4* (accession number AD000671.1) from the four patients were all in intron 3 of the *MLL4* gene (Fig. 1A; Table 1) within or flanked with the Alu repeat sequence (Fig. 1B). As shown in Fig. 1C, full-length viral integration could be expected in HCC131 (g.17752_17753insAB033550.1:g.1827_1826), while truncated virus integrations were detected in the other three tissues, HCC143 (g.17817_17818insAB033550.1:g.2974_1794), HCC146 (g.17514_17515insAB033550.1:g.?_1807), and HCC002 (g.17542_17543insAB033550.1:g.1051_1762). In all four patients, the viral junctions described above were located in the vicinity of DR1, suggesting that the DR1 region is the preferred viral junction for HBV DNA integration.

On Southern blot analysis, clonally integrated HBV DNA sequences were detected in the tumor tissue of HCC131 and a positive control. We encountered the limitations with the heterogeneity of other samples. Using Southern blot hybridization

TABLE 1. Detection of HBV Integration and the Translocation of *MLL4* in HCC

Case no.	Chromosome	Accession no.	Gene	t(17;19)(p11;q13.1)
HCC131	19q13.1	AD000671.1	*MLL4*	Positive
HCC146	19q13.1	AD000671.1	*MLL4*	Positive
	7p14_15	AC005090.2		
HCC002	19q13.1	AD000671.1	*MLL4*	Positive
HCC003	5p13	AY007685.1	*TERT*	Positive
HCC9907	9q13_21.3	AL133578.1		Negative
HCC155				Positive
H20				Positive
H54	18p11.3	AP000845.4	*NMP p84*[a]	Positive
H120				Positive
HCC143	19q13.1	AD000671.1	*MLL4*	Positive
H49				Positive
H62				Negative
H70				Positive
H72				Positive
H78				Positive
H89				Positive
H76				Positive
H57				Negative
H71				Positive
H85				Positive
H86				Negative
H87				Positive
HCC128				Positive
HCC147				Positive
HCC127				Positive
HCC001				Positive
H148				Negative
H149				Negative
H150				Negative
HCC9833				Negative
HCC9901				Negative
HCC9906				Negative

[a]This integration was already reported. Chromosome locations, GenBank accession numbers, and gene names are indicated for eight viral/cellular junctions from seven HCC samples. Detection of t(17;19)(p11;q13.1) was indicated as positive.

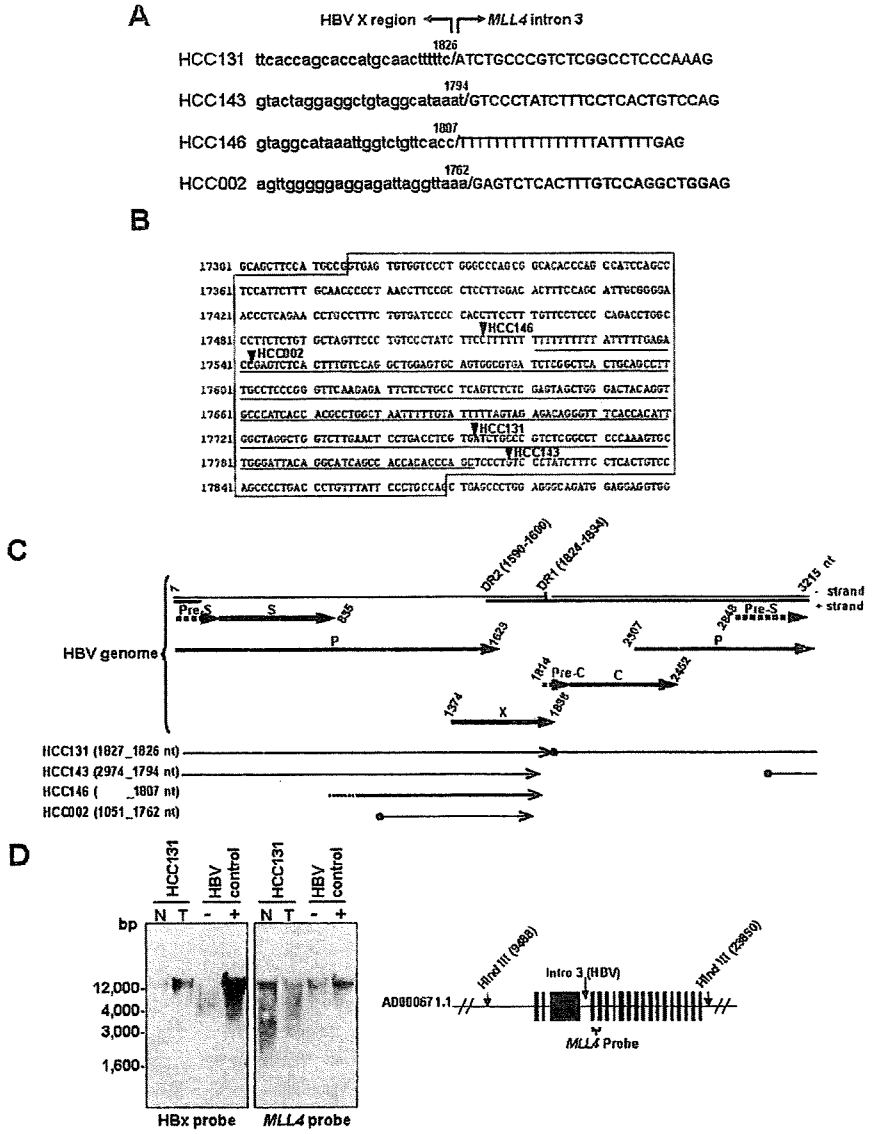

FIGURE 1. **Surrounding sequences of HBV integration sites. A: Sequences of HBV/cellular DNA junctions in the *MLL4* gene in HCC131, HCC143, HCC146, and HCC002. In each sample, the small letters on the left show sequences of the integrated HBV DNA and capital letters on the right show the flanking *MLL4* gene sequences. Numbers above indicate HBV nucleotides at the HBV/cellular DNA junction (Accession number AB033550.1). B: Sequences around intron 3 of the *MLL4* gene and four HBV DNA integration sites are shown. The left side indicates nucleotide positions of *MLL4* gene (accession number AD000671.1). Intron 3 of the *MLL4* gene is indicated by the box (17316_17869 nt). The Alu repeat is shown by underline (17521_17812 nt). C: Schematic representation of gene organization of HBV genome and four integrated HBV genomes (HCC002, HCC131, HCC143, and HCC146). Open reading frames and their directions of transcription are represented by an arrow. The numbers above the arrow indicate location of each open reading frame (Accession number AB033550.1). DR1 and DR2 are the 11 basepair direct repeats. • and > indicate the 5′ and 3′ end of integrated HBV DNA sequences (we could not obtain the 5′ end for HCC146). The lengths of the solid lines represent the size and location of the integrated HBV. D: Southern blot analysis, using the HBx region as probe (left panel) and the *MLL4* probe (right panel). Hind III-digested DNAs from nontumor tissue of HCC 131 (lane 1), tumor tissue of HCC131 (lane 2), colon cancer tissue as negative control (lane 3), and the HBV integrated HCC tissue as positive control (lane 4). Schematic representation for *MLL4* gene and Hind III site are shown. HBV integration site (intron 3) and *MLL4* probe are indicated. Closed boxes indicate exons of *MLL4* gene.**

with an *MLL4* probe of the same membrane, hybridization signals were also detected in the tumor tissue of the patient (Fig. 1D).

HBV Integration Into the *MLL4* Gene Drives Expression of Chimeric Transcripts

In the four HBV/*MLL4* samples, all the integrated viral genome contained HBx promoter and HBx ORF (1374_1838 nucleotides of AB033550.1) except the C-terminus (Fig. 1C). RT-PCR study for detecting fusion transcripts was carried out with HBx primer and reverse primers on various exons of *MLL4* in the four HCC tissues showing various species in each sample (Fig. 2A). In all HCC tissues, in-frame chimeric transcripts that contained exon 4 and exon 5 of *MLL4* were detected (Fig. 2B). In HCC131, two transcripts were observed; one transcript, a major form, showed in-frame fusion containing intron 3 and the other transcript retained intron 4 that led to the creation of the termination codon in exon 6. In HCC002, three transcripts were observed; one transcript

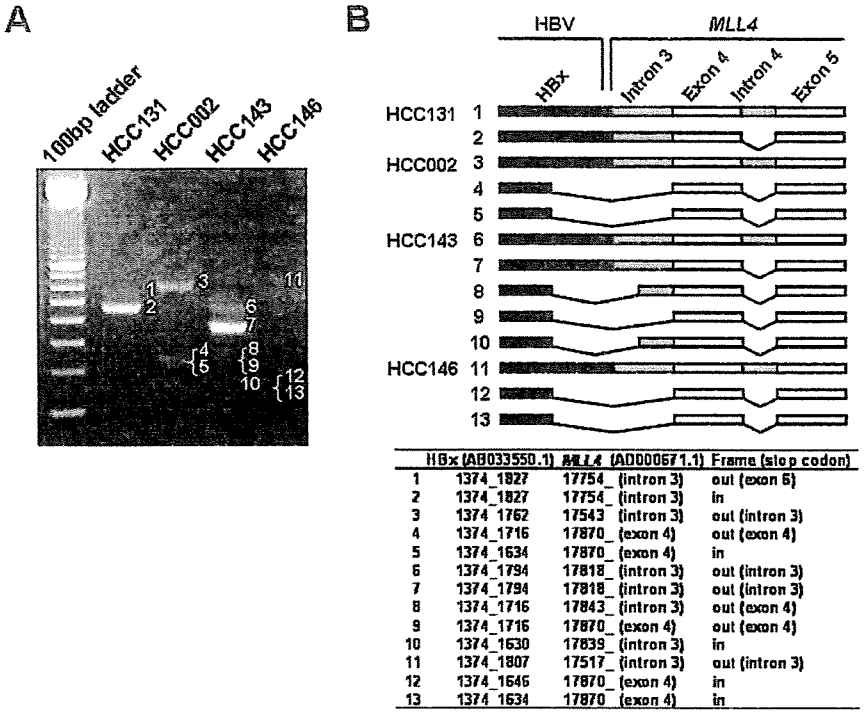

	HBx (AB033550.1)	MLL4 (AD000671.1)	Frame (stop codon)
1	1374_1827	17754_ (intron 3)	out (exon 6)
2	1374_1827	17754_ (intron 3)	in
3	1374_1762	17543_ (intron 3)	out (intron 3)
4	1374_1716	17870_ (exon 4)	out (exon 4)
5	1374_1634	17870_ (exon 4)	in
6	1374_1794	17818_ (intron 3)	out (intron 3)
7	1374_1794	17818_ (intron 3)	out (intron 3)
8	1374_1716	17843_ (intron 3)	out (exon 4)
9	1374_1716	17870_ (exon 4)	out (exon 4)
10	1374_1630	17839_ (intron 3)	in
11	1374_1807	17517_ (intron 3)	out (intron 3)
12	1374_1646	17870_ (exon 4)	in
13	1374_1634	17870_ (exon 4)	in

FIGURE 2. RT-PCR analysis of HBx/*MLL4* fusion transcripts. **A:** Various transcripts were observed for each of the HCC tissues by RT-PCR. **B:** Schematic representation of the fusion transcripts from four HCC tissues (HCC131, HCC002, HCC143, and HCC146), and adjacent sequences between HBx (3′ end) and *MLL4* (5′ end) are summarized. HBx cDNA (black boxes) and *MLL4* gene (exon 4 and 5 as white boxes and intron 3 and 4 as gray boxes) are shown. Spliced out sequences are indicated by bars. Location of 5′ end of *MLL4* in intron 3 or exon 4 is also shown. Reading frame based on HBx cDNA followed by *MLL4* is indicated for individual chimeric transcripts. Location of the aberrant stop codon is also shown except for in-frame transcripts. See the Supplementary Appendix for more information.

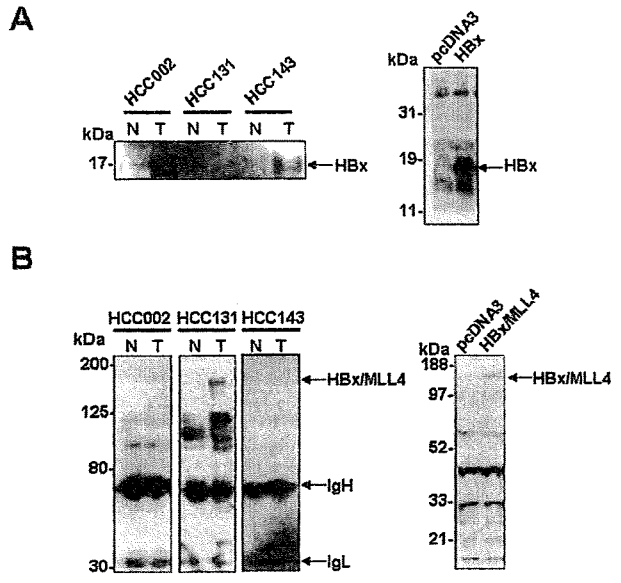

FIGURE 3. **Immunodetection of HBx fusion proteins in HCC samples. A:** Western blot analysis of tumor tissues (T) from HCC002, HCC131, and HCC143 and the adjacent nontumor tissues (N) by using the monoclonal anti-HBx antibody. Recombinant full-length HBx protein expressed in HepG2 cells are also shown. **B:** Immunoprecipitation followed by immunodetection with HBx antibody detected HBx/MLL4 putative fusion protein specifically in HCC131 T (left panel). Western blot using Flag antibody detected an approximately 170-kDa HBx/MLL4 fusion protein transiently expressed in HepG2 cells (right panel). See the Supplementary Appendix for more information.

retained intron 3 causing premature termination and the other two transcripts spliced out intron 3 using distinct 5′ splice sites, resulting in one transcript (nucleotide position 261) showing the in-frame transcript and the other (nucleotide position 343) the premature termination. Similar patterns were observed for HCC146. In HCC143, five species were observed, and the splicing junction of the in-frame transcript was CC-GT, and does not conform to the GT-AG rule.

HBx-MLL4 Fusion Proteins Expressed in HCC

To confirm that the fusion transcripts were translated, the expression of HBx-related proteins in the tumor and adjacent liver tissues were tested by immunodetection with an antibody against HBx protein. Western blot analysis showed that an approximately 17-kDa protein, which represents a short HBx fusion protein compared to recombinant full-length HBx protein expressed in HepG2 cells, is selectively expressed in the HCC002 and HCC143 tumor tissues (Fig. 3A). Immunoprecipitation followed by Western blot analysis detected an approximately 170-kDa protein in HCC131 (Fig. 3B). We constructed an expression vector that can express fusion protein consisting of N-terminally Flag-tagged HBx ORF (amino acids 1_154) and *MLL4* coding region beginning from exon 4 (corresponding to amino acids 820_2715, accession number NM_014727.1), and transiently expressed into HepG2 cells. Western blot using Flag antibody clearly detected an approximately 170-kDa protein (Fig. 3B, right panel). MLL is known to be cleaved at a conserved site and this cleavage generates N- and C-terminal fragments [Hsieh et al., 2003]. MLL4 also possesses a conserved site D/GVDD (amino acids

TABLE 2. cDNA Microarray Results Showing Upregulation and Downregulation by HBx, HBx/*MLL4* Fusion, and Truncated HBx (1_87aa) Proteins*

	Gene description	Category	HBx		HBx/MLL4		HBx 1_87aa	
			Mean	SD	Mean	SD	Mean	SD
Upregulated gene name								
OR11A1	Olfactory receptor, family 11, subfamily A, member 1	G protein-coupled receptor	3.99	0.02	—		—	
OPN4	Opsin 4 (melanopsin)	G protein-coupled receptor	3.52	0.1	—		—	
UPB1	Ureidopropionase, beta	Hydrolase	3.09	0.52	—		3.89	2.2
HIST1H4L	H4 histone family, member K	Nucleosome structure	3.08	0.3	—		2.72	0.3
HIST1H4I	H4 histone family, member M	Nucleosome structure	2.8	0.02	—		—	
ELL3	Elongation factor RNA polymerase II-like 3	Transcriptional regulation	2.59	0.06	—		—	
BAI1	Brain-specific angiogenesis inhibitor 1	Cell adhesion	2.57	0.62	—		—	
CEP290	Centrosomal protein 290kDa	Centrosomal protein	2.51	0.66	—		—	
HIST1H4B	H4 histone family, member I	Nucleosome structure	2.38	0.01	—		—	
CDC2L1	Cell division cycle 2-like 1	Cell cycle	2.36	0.4	—		2.36	0.04
OR2C1	Olfactory receptor, family 2, subfamily C, member 1	G protein-coupled receptor	2.15	0.15	—		—	
DNCL2B	Dynein, light chain 2B	Motor protein	2.11	0.04	—		—	
ZNF354B	Zinc finger protein 354B	Transcriptional regulation	2.09	0.06	—		—	
MLL4	Mixed-lineage leukemia 4	Transcriptional regulation	—		31	3.25	—	
Downregulated								
AVIL	Advillin	Actin-binding protein	3	0.42	5.2	1.46	3.51	0.68
ENO2	Enolase 2	Hydratase	2.19	0.21	—		—	
KERA	Keratocan	Extracellular matrix	—		4.91	1.37	—	
UBXD1	UBX domain containing 1	Unknown	—		4.76	0.34	—	
PIAS3	Protein inhibitor of activated STAT3	Signal transduction	—		4.68	0.45	—	
MYBPC2	Fast-type myosin binding protein C	Unknown	—		4	0.48	2.48	0.12
PITPNM	Phosphatidylinositol-transfer protein membrane-associated	Cytokinesis	—		3.58	0.83	—	
EHD2	EH-domain containing 2	Endocytosis	—		3.4	0.43	—	
GJB1	Connexin 32	Gap junction	—		3.01	0.62	—	
WASL	Wiskott-Aldrich syndrome-like	Actin polymerization	—		2.48	0.22	—	
TNRC6C	Trinucleotide repeat containing 6c	Unknown	—		2.31	0.28	—	
TBC1D10B	TBC1 domain family, member 10B	Unknown	—		2.19	0.08	—	

*The experiments were performed twice, and the mean and standard deviation (SD) values were determined for each gene.

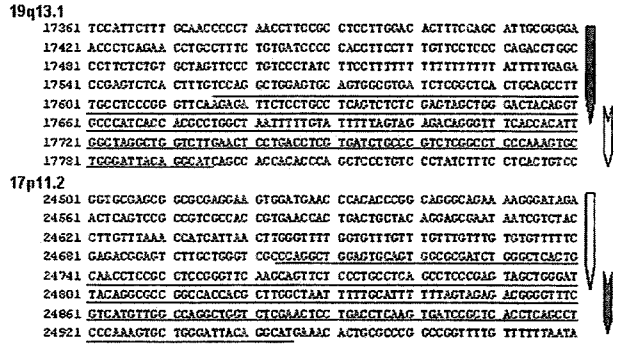

FIGURE 4. **Reciprocal translocation found in intron 3 of the *MLL4* locus. Chromosomal rearrangement between chromosome 19q13.1 (accession number AD000671.1) and chromosome 17p11.2 (accession number AC087294.18) are shown. The sequences of Alu elements are underlined. The downward pointing arrows on the respective chromosomes indicate the newly synthesized chromosomes (black-to-black and white-to-white) after the recombination events occurred via Alu elements.**

2062_2066), indicating a 170-kDa protein could be a posttranslationally modified product.

Functional Elucidation of HBx/MLL4 Fusion Protein by DNA Microarray

To provide mechanistic insights into molecular etiology such as altered target gene expression regulated by HBx/MLL4 fusion protein, we transiently overexpressed full-length HBx and HBx/MLL4 fusion proteins in HepG2 cells. We employed cDNA microarray technology and identified 13 genes that were upregulated and two genes that were downregulated by HBx protein (Table 2). In contrast, no gene (except for *MLL4* itself) was upregulated and 11 genes were downregulated by HBx/MLL4 fusion protein (Table 2). Uniquely, only one gene, Advillin (*AVIL*) was identified as a common target between HBx and HBx/MLL4 fusion proteins. We checked whether C-terminally truncated HBx protein (amino acids 1_87) could regulate the expression of genes identified by above experiments, because HBx protein in HCC002 and HCC143 only had N-terminal 87 and 86 amino acid residues. Three genes were upregulated and two genes, including *AVIL*, were downregulated by truncated HBx protein (Table 2). Taken together, these data predict that HBx/MLL4 fusion protein would suppress the expression pattern of specific genes.

Alu-Mediated Chromosomal Translocation of *MLL4* to 17p11.2 in HCC

We extended the search for HBV DNA integration into intron 3 of the *MLL4* gene in other HCC samples positive for anti-HBc antibody (Supplementary Table S2). The sequencing analyses failed to detect HBV/*MLL4* DNA sequences, instead demonstrated chimeric sequences between the *MLL4* gene and a particular region of chromosome 17p11.2 (Fig. 4). We detected 22 translocations from 32 HCC samples (Table 1). The sequencing analyses of the translocation products revealed an about 240-bp region at the junction that is highly shared by two chromosomes (approximately 85%) containing Alu elements, suggesting that Alu-mediated homologous recombination facilitated translocation (Fig. 4).

DISCUSSION

The classical mechanism by which tumor-associated viruses contribute to oncogenesis is activation of cellular genes with oncogenic potential through viral genome integration into the cellular genome. HBV genome integration into *SERCA1* (sarco/endoplasmic reticulum calcium ATPase) have been demonstrated [Chami et al., 2000]. The resultant chimeric HBx/SERCA1 protein proposed to be implicated in oncogenesis via an apoptotic

mechanism [Chami et al., 2000]. Reports from two groups, including our observation, demonstrate that the promoter region of the *TERT* gene is targeted by HBV in several HCC tissues [Ferber et al., 2003; Paterlini-Brechot et al., 2003]. Therefore, the *TERT* gene most likely serves as a nonrandom integration site of the viral genome in a subset of HBV-positive HCCs, and the oncogenic HBV DNA integrations may possess the preferential sites. In this study, we further demonstrated four cases of integrations into the *MLL4* gene in HBsAg-positive HCC samples. Sequencing analyses revealed that all of the host sites were within 300 bp of intron 3, flanked with the Alu element of the *MLL4* gene. Recently, HBV DNA integration into *MLL4* gene in three Japanese HCC patients, two cases into exon 3 integration and one into intron 3, were reported [Tamori et al., 2005]. These results support the hypothesis that the oncogenic viral integrations into hepatocytes are not entirely random.

HBV integration into intron 3 of *MLL4* resulted in several fusion transcripts between HBx and *MLL4* that could be directly implicated in liver oncogenesis, albeit the C-terminally truncated HBx protein, as observed in HCC002 and HCC143, might be more closely related to oncogenesis. Our cDNA microarray experiments indicate that HBx/MLL4 fusion protein suppressed the unique genes. It might be speculated that the fusion gene product lacking an AT hook, which is encoded in exons 1–3 of *MLL4*, is directly related to oncogenesis. Further investigation of HBx/MLL4-dependent or N-terminal MLL4-dependent transcriptional regulation may provide a novel insight into the elucidation of etiology of hepatic oncogenesis.

The *MLL4* gene, originally reported as a second human homolog of the *MLL* gene, is mapped to chromosome 19q13.1 [FitzGerald and Diaz, 1999], where gene amplification was reported in HBV-related HCCs [Marchio et al., 1997; Huntsman et al., 1999] and frequent genome rearrangements in solid tumor were reported [Curtis et al., 1998]. We detected the chromosomal translocation of the *MLL4* locus to chromosome 17 in 22 tumors out of 32 samples. The chromosomal rearrangement occurred between intron 3 of the *MLL4* gene of chromosome 19q13.1 and chromosome 17p11.2. The two chromosomal regions share nearly identical Alu elements, indicating that Alu-mediated recombination most likely explains the genome rearrangement. HBV infection and subsequent hepatitis induced DNA damage such as double-strand breaks [Dandri et al., 2002; Bill and Summers, 2004]; therefore, the genome repair mechanism is essential for maintaining the genome integrity and cellular viability.

In conclusion, we detected the translocation breakpoint point in the intron 3 of *MLL4* gene that provides one of the preferential targets for HBV integrations. Indeed we also found recurrent integrations of HBV DNA into intron 3 of *MLL4* gene in four HCC cases, and chimeric HBx/*MLL4* transcripts and HBx/MLL4 proteins, suggesting that the insertional mutagenesis could be functionally relevant to liver oncogenesis.

ACKNOWLEDGMENTS

We are grateful to Dr. Murakami (National Cancer Center Research Institute, Japan) and Dr. Miyamura, Dr. Suzuki, and Dr. Shoji (National Institute of Infectious Disease, Japan) for their technical support and helpful comments. This work was partly supported by grant from the CREST of Japan Science and Technology (II) to I.I.

REFERENCES

Bill CA, Summers J. 2004. Genomic DNA double-strand breaks are targets for hepadnaviral DNA integration. Proc Natl Acad Sci USA 101:11135–11140.

Block TM, Mehta AS, Fimmel CJ, Jordan R. 2003. Molecular viral oncology of hepatocellular carcinoma. Oncogene 22:5093–5107.

Brechot C, Gozuacik D, Murakami Y, Paterlini-Brechot P. 2000. Molecular bases for the development of hepatitis B virus (HBV)-related hepatocellular carcinoma (HCC). Semin Cancer Biol 10:211–231.

Chami M, Gozuacik D, Saigo K, Capiod T, Falson P, Lecoeur H, Urashima T, Beckmann J, Gougeon ML, Claret M, le Maire M, Brechot C, Paterlini-Brechot P. 2000. Hepatitis B virus-related insertional mutagenesis implicates SERCA1 gene in the control of apoptosis. Oncogene 19:2877–2886.

Curtis LJ, Li Y, Gerbault-Seureau M, Kuick R, Dutrillaux AM, Goubin G, Fawcett J, Cram S, Dutrillaux B, Hanash S, Muleris M. 1998. Amplification of DNA sequences from chromosome 19q13.1 in human pancreatic cell lines. Genomics 53:42–55.

Dandri M, Burda MR, Burkle A, Zuckerman DW, Will H, Rogler CE, Greten H, Petersen J. 2002. Increase in de novo HBV DNA integrations in response to oxidative DNA damage or inhibition of poly(ADP-ribosyl)ation. Hepatology 35:217–223.

Ferber MJ, Montoya DP, Yu C, Aderca I, McGee A, Thorland EC, Nagorney DM, Gostout BS, Burgart LJ, Boix L, Bruix J, McMahon BJ, Cheung TH, Chung TK, Wong YF, Smith DI, Roberts LR. 2003. Integrations of the hepatitis B virus (HBV) and human papillomavirus (HPV) into the human telomerase reverse transcriptase (hTERT) gene in liver and cervical cancers. Oncogene 22:3813–3820.

FitzGerald KT, Diaz MO. 1999. MLL2: a new mammalian member of the trx/MLL family of genes. Genomics 59:187–192.

Gozuacik D, Murakami Y, Saigo K, Chami M, Mugnier C, Lagorce D, Okanoue T, Urashima T, Brechot C, Paterlini-Brechot P. 2001. Identification of human cancer-related genes by naturally occurring hepatitis B virus DNA tagging. Oncogene 20:6233–6240.

Hsieh JJ, Ernst P, Erdjument-Bromage H, Tempst P, Korsmeyer SJ. 2003. Proteolytic cleavage of MLL generates a complex of N- and C-terminal fragments that confers protein stability and subnuclear localization. Mol Cell Biol 23:186–194.

Huntsman DG, Chin SF, Muleris M, Batley SJ, Collins VP, Wiedemann LM, Aparicio S, Caldas C. 1999. MLL2, the second human homolog of the Drosophila trithorax gene, maps to 19q13.1 and is amplified in solid tumor cell lines. Oncogene 18:7975–7984.

Marchio A, Meddeb M, Pineau P, Danglot G, Tiollais P, Bernheim A, Dejean A. 1997. Recurrent chromosomal abnormalities in hepatocellular carcinoma detected by comparative genomic hybridization. Genes Chromosomes Cancer 18:59–65.

Mitelman F, Mertens F, Johansson B. 1997. A breakpoint map of recurrent chromosomal rearrangements in human neoplasia. Nat Genet 15:417–474.

Paterlini-Brechot P, Saigo K, Murakami Y, Chami M, Gozuacik D, Mugnier C, Lagorce D, Brechot C. 2003. Hepatitis B virus-related insertional mutagenesis occurs frequently in human liver cancers and recurrently targets human telomerase gene. Oncogene 22:3911–3916.

Siebert PD, Chenchik A, Kellogg DE, Lukyanov KA, Lukyanov SA. 1995. An improved PCR method for walking in uncloned genomic DNA. Nucleic Acids Res 23:1087–1088.

Tamori A, Yamanishi Y, Kawashima S, Enomoto M, Tanaka H, Kudo S, Shiomi S, Nishiguchi S. 2005. Alteration of gene expression in human hepatocellular carcinoma with integrated hepatitis B virus DNA. Clin Cancer Res 11:5821–5826.

Cell Transplantation, Vol. 17, pp. 51–59, 2008
Printed in the USA.

0963-6897/08 $90.00 + .00
E-ISSN 1555-3892
www.cognizantcommunication.com

A Newly Developed Immunoisolated Bioartificial Pancreas With Cell Sheet Engineering

Jeong Ik Lee,*† Ryohei Nishimura,* Hideaki Sakai,‡ Nobuo Sasaki,* and Takashi Kenmochi†

*Laboratory of Veterinary Surgery, Graduate School of Agricultural and Life Sciences, University of Tokyo, Tokyo, Japan
†Clinical Research Center, Chiba-East National Hospital, National Hospital Organization, Chiba, Japan
‡CellSeed Inc., Tokyo, Japan

The term "immunoisolation" refers to the encapsulation of a graft in a selectively permeable membrane. Encapsulation of cellular grafts may provide a way to protect the graft from immune attack without the need for immunosuppressive agents. Although numerous types of artificial materials have been used for encapsulating membranes, their incomplete biocompatibility causes foreign body reaction against the membranes. A new technique has been developed, called cell sheet engineering using temperature-responsive culture dishes, that allows the use of living cells as an immunoisolating membrane in this study. Using this method, the cultured cells can be easily harvested in the shape of a sheet by a simple change of the temperature without the use of proteolytic enzymes. A cell sheet can be created with three-dimensional structure by making multiple cell sheet layers. In this study, a new technique of macroencapsulation (bioartificial organs) has been developed using chondrocyte sheets. Among the various candidate cells, pancreatic islet cells were selected for a bioartificial organ in this study. A chondrocyte sheeting immunodelusive immunoisolated bioartificial pancreas (CSI-BAP) was manufactured by means of cell sheet engineering. An auricular cartilage, which is a histologically elastic cartilage from dogs (beagle), was used as a source of immunoisolating membrane. CSI-BAP was made by multilayering the chondrocyte sheets, and the donor's islets were located between each sheet. Islets were isolated and prepared from the dog (ALLO-model) and Brown Norway (BN) rat (XENO-model). The CSI-BAP was cultured for 83 days and the cultured medium was collected every 24 h to measure the insulin concentrations. The CSI-BAP was examined histologically using hematoxyhin and eosin (H&E), and azan dye staining. In addition, immunohistochemical staining was performed to demonstrate the insulin production of CSI-BAP. Insulin secretion of CSI-BAP on day 16 was reduced to 21.4% of the insulin secretion level of day 10, which was the start point of measurement. Although a gradual reduction was observed, insulin secretion was maintained for 3 months. The CSI-BAP was capable of secreting insulin to the culture medium during the observation period. Histological evaluations demonstrated the good viability of the islets, and immunohistochemistry showed the positive staining of insulin. This novel technology may be used for other kinds of endocrine cells or hepatocytes, which may become the models for immunoisolated bioartificial organs in the near future.

Key words: Bioartificial organ; Auricular chondrocyte; Islet; Cell sheet engineering; Maroencapsulation; Immunoisolation

INTRODUCTION

Immunoisolation has been achieved by encapsulating the graft cells using selectively permeable membranes. Such membranes only allow the permeation of smaller molecules, such as oxygen, CO_2, glucose, amino acids, and hormones, but prevent the penetration of immunocytes and larger immune molecules, such as antibodies and complements. Although many kinds of artificial materials have been used for the membranes during the past few decades (4,5,13,15,16,18,23), they are not sufficiently biocompatible and thus cause a foreign body reaction and fibrosis (13,15). If the immunoisolating method of macroencapsulating is properly used, bioartificial organs can be the technological key to transplantation without immunosuppression (24).

In contrast, a cartilage is a natural tissue that lacks blood vessels, lymph vessels, and nerves, and uses diffusion for allowing adequate exchanges of nutrients and waste as well as oxygenation. So it is impossible for leukocytes to penetrate into the normal cartilage (6). Chondrocytes in cartilage are surrounded with extracel-

Received February 5, 2007; accepted September 30, 2007.
Address correspondence to Takashi Kenmochi, M.D., Ph.D., Clinical Research Center, Chiba-East National Hospital, National Hospital Organization, 673 Nitonacho, Chuo-ku, Chiba-city, Chiba, 260-8712, Japan. Tel: +81-43-261-5171, Ext. 2700; Fax: +81-43-268-2613; E-mail: kenmoti@nitona.hosp.go.jp

lular matrix (ECM; e.g., collagens and proteoglycan), which is produced by the chondrocyte itself. Moreover, because the auricular cartilage is an elastic cartilage, it has elasticity property and is easy to collect from patients. This suggests that cartilage can be used as an ultimate and versatile membrane for immunoisolation, if chondrocytes can be harvested in the shape of a membrane and cover the graft cells completely.

As a result of recent progress in tissue engineering (10), researchers can now use many techniques for the in vitro handling of vital tissues and cells. Cell sheet engineering, which is based on the technique of nanobiointerface, is one of the prospective methods among the newly developed tissue engineering technologies (1,7, 20,22,29,30). It could be a great source of immunoisolating membrane, if chondrocyte sheets are manufactured and harvested by this technique. For the first application of the immunoisolation using the chondrocyte sheet method, pancreatic islets were used in this study.

Islet transplantation has been clinically performed for patients with insulin-dependent type 1 diabetes mellitus (IDDM) instead of a conventional insulin injection treatment. However, there are many problems to be solved including a shortage of donor organs. Another factor that may contribute to a lower success rate of islet transplantation in type 1 diabetic patients is the side effects of the immunosuppressive drugs. Although every recipient has to take these expensive drugs after islet transplantation to avoid rejection by the attack of their own immune system, these drugs have some serious side effects (19). Furthermore, the function of islet cells may be diminished by the direct toxicity of immunosuppressive drugs to the beta cells (26).

The purpose of this study was to prospectively evaluate long-term function of CSI-BAP in vitro, and to investigate the structure of CSI-BAP and its relationship between chondrocyte sheets and islets.

MATERIALS AND METHODS

Islet Isolation and Purification Procedure

Pancreatic islets were prepared using the technique described previously (25) with some modifications. Pancreata from Brown Norway (BN) rats (males, 250 ± 50 g, SLC Japan Co., Hamamatsu, Japan) and dogs (beagle, 12–24 months old, body weight 9–13 kg) were expanded with Hank's balanced salt solution (HBBS) containing 10 mmol/L HEPES plus 2.0 mg/ml cold collagenase (Collagenase P, Roche Applied Science Co., Germany) and 5% heat-inactivated fetal bovine serum (FBS: JRH Biosciences, Lenexa, KS, USA) by the ductal injection. Subsequently, the distended pancreas was mixed with a Vortex Genie 2 (Scientific Industries, Bohemia, NY, USA) for a while , and then it was digested by shaking in a water bath at 37°C for 16 min (for rat) or 45 min (for dog), respectively. The resulting cell suspensions were passed through a 600-μm steel mesh filer. Islets were purified by Histopaque (Sigma Chemical Co., St. Louis, MO, USA) density gradients. Rat islets were collected and hand-picked twice for purification. The islet number was determined by counting the triple samples of each batch of islet preparations. Islets were counted and their diameters were measured after staining with diphenylthiocarbazone (dithizone: Sigma Chemical Co.). Islets were cultured in the mixed culture medium (MCM) containing 50% Ham's F-12 medium (Invitrogen Co., Carlsbad, CA, USA) and 50% RPMI-1640 without glucose (Invitrogen Co.) with plus 25 mmol/L HEPES, 1% antibiotic/antimycotic mixture (ABAM; 10,000 U/ml penicillin G, 10,000 μg/ml streptomycin sulfate, and 25 μg/ml amphotericin B as Fungizone®; Invitrogen Co.), and 50 μg/ml ascorbic acid (Sigma Chemical Co.). The final concentration of heat-inactivated FBS was adjusted to 10% and the glucose concentration was adjusted to 100 mg/dl by adding D-(+)-glucose (Sigma Chemical Co.).

Primary Culture of Chondrocytes From Auricular Cartilage

Auricular cartilage was obtained from dogs. The specimens, which were stripped of their surrounding tissue, including the skin, subcutaneous fat tissue, muscles, and perichondrium, were cut into small pieces. The cartilage was cut using scissors with curved blades on a special glass dish (12 cm diameter, Toshin-Riko Co., Japan). Cartilage tissue was cut into small pieces (~0.5-mm cubes) in a short time. Thereafter, the chondrocytes were digested in the cocktail solution of Ham's F-12 medium (Invitrogen Co.) plus 0.3% collagenase (Collagenase class II: Worthington, Biochemical Co., Lakewood, NJ, USA), 0.25% trypsin (Invitrogen Co.), 4% ABAM, and 50 μg/ml ascorbic acid in a shaking water bath at 37°C overnight. The cell suspension was passed through a 70-μm and a 40-μm nylon cell strainer (BD Falcon™; BD Biosciences, Bedford, MA, USA), and the isolated cells were washed twice with phosphate-buffered saline (PBS; Invitrogen Co.) containing 4% ABAM, and the viable cells were counted on Burker-Turk hematocytometer with a trypan blue staining. These chondrocytes were seeded and expanded by the sequential passages (passage 1–3) in monolayer culture in CBM™ medium (Cambrex Bio Science, Walkersville, MD, USA) supplemented with CGM SingleQuot® (Cambrex Bio Science), and 50 μg/ml ascorbic acid, and maintained at 37°C in humid 5% CO_2. The chondrocytes at passage 1 were plated at a cell density of $0.5 \times 10^4/cm^2$. Passages 2–3 were subsequently reseeded at a density of $0.25 \times 10^4/cm^2$. The culture medium was changed twice a week. To manufacture CSI-BAP, only cells recovered from

passage 3 cells were used as a macroencapsulating source of sheets.

Manipulation of Chondrocytes Sheets Into Layered Constructs for CSI-BAP

Cells recovered from passage 3 of the chondrocyte culture were used for constructing the cell sheets. Expanded to passage 3, the elastic chondrocytes were plated onto 60-mm plates made of the temperature-responsive polymer, poly(*N*-isopropylacrylamide) (PIPAAm), pattern-grafted dishes (Upcell™; Cellseed, Co., Tokyo, Japan) at a seeding density of $1.5–2.0 \times 10^4/cm^2$, and cultured in the growth medium until they reached 100% confluency. The culture medium was changed twice a week for 3–6 weeks until the cell sheets were harvested. At 100% confluency, the chondrocytes were detached from the dish and multilayered using the previously described technique (7,20,21) with a little modification. The procedure for three-dimensional manipulation of cultured chondrocyte sheets and the process that produces CSI-BAP is shown in Figure 1. Briefly, to release confluent cells as a cell sheet, the culture dishes were located in a clean bench at room temperature around 24°C, and the sheets were detached spontaneously from the dish surfaces within 30 min. In order to preserve cell sheet morphology without shrinking, hydrophilically modified poly(vinylidene difluoride) (PVDF) membranes (Millipore, Bedford, MA, USA) were used as supporting membranes. The supporting membranes, which were cut to fit Upcell™, were placed directly over the confluent chondrocytes. The lifting cell sheet edges promptly attached to the overlaid PVDF membranes, and the membrane–cell sheet films gently were peeled off Upcell™ with forceps. These cell sheets physically attached to the PVDF membranes were transferred onto other confluent chondrocytes sheets. Double-layered cell sheets were then incubated at 37°C for 30 min in a minimum amount of culture medium to attach the newly transferred cell sheets to the basal cell sheets. Then additional culture medium was added and the dish was incubated again at 37°C. By repeating this procedure, the chondrocyte multilayer sheets were finally obtained. From three to five layered chondrocyte sheets were used to fabricate a CSI-BAP. Subsequently, CSI-BAP was made by unifying the two multilayered chondrocyte sheets and layering the donor's islets between each multilayer sheet. The CSI-BAP was then incubated at 37°C for 30 min in a small amount of medium to attach the opposite side of chondrocyte sheets to cover basal sheets on which isolated islets were placed. Then culture medium was added and the culture dishes were incubated again at 37°C. To obtain firm and perfect integration of the cells in the CSI-BAP including pancreatic islets and chondrocyte sheets, the CSI-BAP was incubated under ordinary culture conditions (37°C and 5% CO_2) with MCM for 7–10 days. Islets prepared from dog (ALLO-model) and the BN rat (XENO-model) were used for CSI-BAP. The ALLO-model of CSI-BAP was kept in culture for 3 months, and the XENO-model was used for histological analysis.

Measurement of Insulin Secretion

CSI-BAP was maintained in the culture media at 37°C in humid 5% CO_2 using MCM for 83 days. MCM was changed every 24 h and the medium samples were immediately frozen at −80°C until measurement. The supernatants were collected and the insulin content was determined using a microparticle enzyme immunoassay (MEIa) (IMx Insulin, Abbot Laboratories, Tokyo, Japan).

Histological Studies

The CSI-BAP was fixed in 4% paraformaldehyde. After washing with PBS (Invitrogen Co.) it was embedded in paraffin. Subsequently, the CSI-BAP was sectioned and stained with hematoxylin and eosin (H&E) and azan staining for histological evaluation. The samples were also analyzed by immunohistochemistry for insulin using the avidin-biotin-peroxidase complex technique according to the manufacturer's protocol (LSAB 2 kit/HRP, DAKO Japan Co., Ltd.) using 3-amino-9-ethylcarbazole (AEC) substrate-chromogen solution (DAKO Japan Co., Ltd.).

RESULTS

Islet Yield

Dog islets were obtained from one fourth of the whole pancreas, which resulted in an approximately 7-ml pellet after digestion. The final average of yield was 32,447.56 islet equivalent (25,920 raw number) and the purity was approximately 85%. The average number of islets isolated from one pancreas per BN rat was 1792.11 islet equivalent (1464.38 raw number) and the purity was 99%.

Primary Culture of Chondrocytes From Auricular Cartilage

The number of chondrocytes from 1 g of auricular cartilage was an average of 351.25×10^4. The chondrocytes expanded from 15,046 to 129,377 during three passages. The chondrocytes were cryopreserved at every passage and they were thawed to use for the experiment. The recovery rate of frozen–thawed chondrocytes was $51.01 \pm 4.44\%$.

Morphological Studies of CSI-BAP

Chondrocyte sheets were prepared and combined to form three to five layers (Fig. 1). The confluent chondrocytes could be harvested noninvasively as the contig-

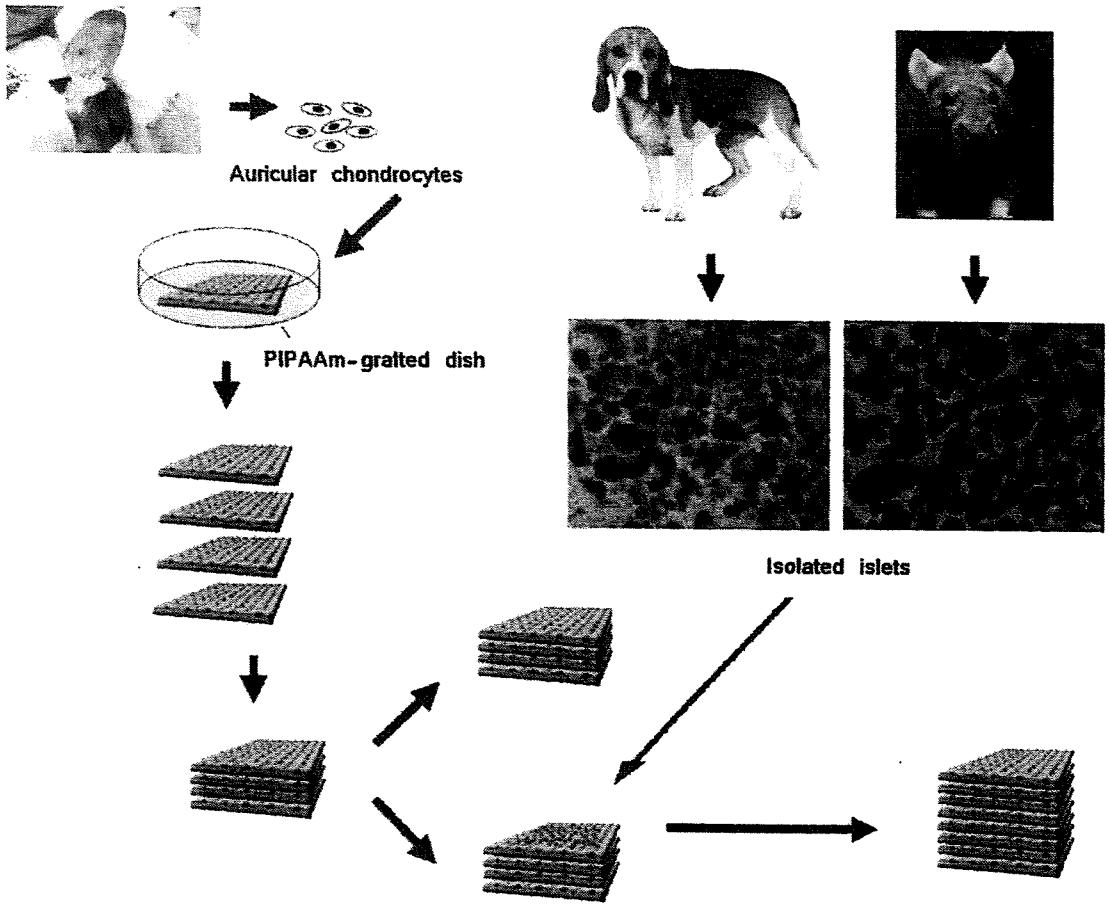

Figure 1. Schematic illustration of the manufacture of chondrocyte sheeting immunoisolated bioartificial pancreas (CSI-BAP). Confluently cultured chondrocytes were incubated at room temperature around 24°C, and the sheets began to detach spontaneously from the dish surfaces within 30 min. The detached chondrocyte sheet was transferred and piled onto another chondrocyte sheet and incubated at 37°C, yielding bilayer chondrocyte sheets. By repeating this process, multilayer sheets (3–10 layers) could be formed. Subsequently, CSI-BAP was made by unifying two multilayered chondrocyte sheets and then transferring the donor's islets in between the multilayer sheets.

uous cell sheets with intact cell–cell junctions and deposited extracellular matrix (ECM). Because the ECM associated with the basal side of the cell sheets shows adhesion, the harvested cell sheets could be stratified to reconstruct thicker or more complex tissue architectures. Confluent chondrocytes cultured were incubated at room temperature, and the sheets began to detach spontaneously from the dish surfaces. The detached chondrocytes sheet was transferred and piled onto another chondrocyte sheet, yielding bilayer chondrocyte sheets. Technically, it was possible to stack up to 10 sheets of chondrocytes (Fig. 2).

To fabricate CSI-BAP, it was necessary to unify the two multilayered chondrocyte sheets and to place donor islets between each multilayer sheet. For the XENO-model of CSI-BAP, two three-layered sheets and islets obtained from 1 to 6 rats were used. In contrast, in the ALLO-model, two five-layered sheets were used with the islets (46,000 islet equivalent, 64,800 raw number). Figure 3 shows the histological appearance of CSI-BAP with H&E (Fig. 3A) and azan staining (Fig. 3B). The well-formed and round-shaped islets were observed in the sheet, which demonstrated the preservation of the islet structure in the sheet in this study. In addition, there was positive staining of insulin with immunohistochemistry (Fig. 3C), thus suggesting a good endocrine function of the islets. Using azan staining, the islets were clearly detected in the multilayered chondrocyte sheets (Fig. 3B). The application of the "azan" staining to mammalian islet differentiates sharply the type of cells, including A, B, and D cells. A cells were shown as red granules, B cells as orange-gray, and D cells as blue (2).

From these data, it was demonstrated that completely viable pancreatic islets were maintained in the layered chondrocytes sheets.

Insulin Measurement

The insulin secretion from CSI-BAP was positively detected during the entire observation time of 83 days (Fig. 4). The amount of insulin gradually decreased from the first day of the insulin measurement, which was at day 10 in culture. Insulin release of CSI-BAP on day 16 decreased to 21.4% of insulin secretion level of day 10 (Table 1). After day 16, the insulin secretion was comparatively preserved until 83 days. Islets in CSI-BAP were capable of secreting insulin through the observation period, indicating that insulin was released from the islets in CSI-BAP by diffusion.

DISCUSSION

An immune reaction begins upon recognition of self and nonself. Allogenic or xenogenic grafts are recognized to be nonself and will be rejected in the case of transplantation. Immunosuppression is, thus, necessary to maintain the transplanted grafts. Various problems still exist regarding immunosuppression. One of the major problems of immunosuppressive drugs is that these agents focus not only on the transplanted grafts but also on the entire host immune system of the recipients. The patients must take drugs to prevent the rejection of the

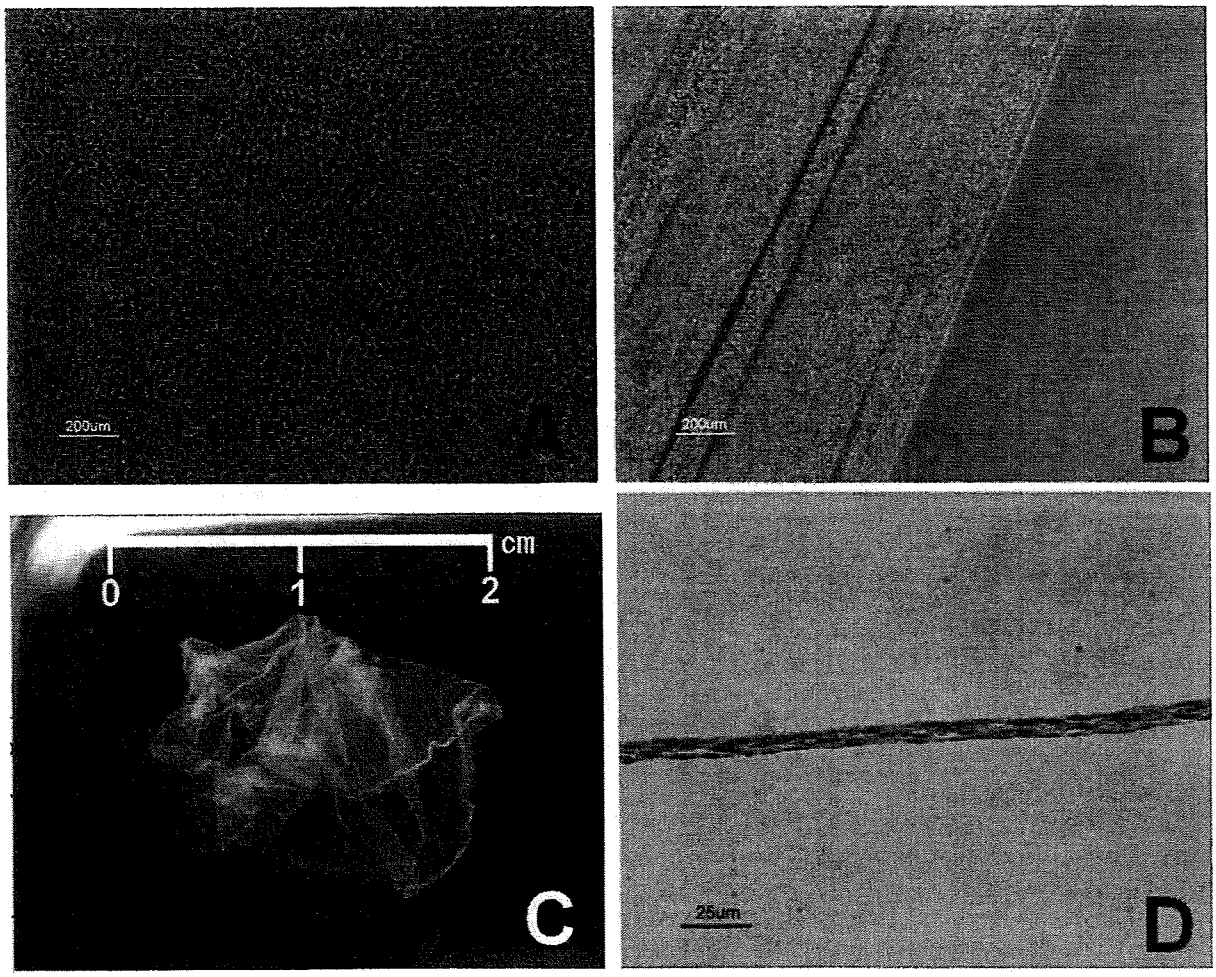

Figure 2. Chondrocyte sheet. Phase-contrast micrograph (A, B) of auricular chondrocyte sheet that is now being detached from temperature-responsive culture dishes (Upcell™; PIPAAm-grafted cell culture dishes). (A) Confluently cultured chondrocytes are spontaneously and gradually detached (B) when the temperature is reduced below 32°C, without the need for proteolytic enzymes. (C) The confluent cells are noninvasively harvested as single, contiguous cell sheets with intact cell–cell junctions and deposited ECM. Because the ECM associated with the basal side of the cell sheets shows adhesion, the harvested cell sheets can be stratified to construct thicker or more complex tissue architectures. (D) Four-layered chondrocyte sheet stained with hematoxylin and eosin.

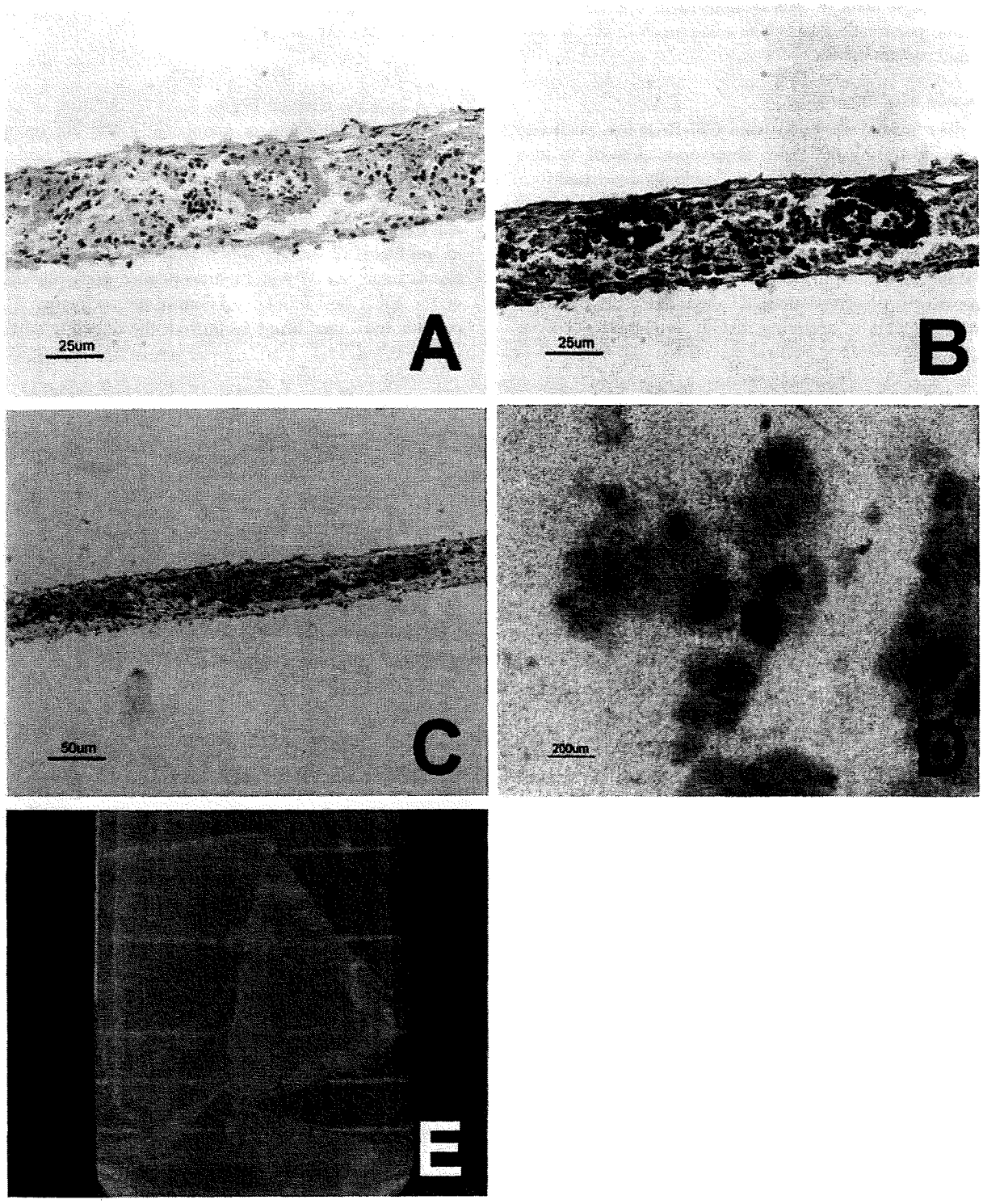

Figure 3. CSI-BAP. A histological evaluation with hematoxylin and eosin stain (A), azan dye (B), and immunohistochemistry for insulin (C) confirmed insulin secretion within the beta cells of pancreatic islets, showing that the islets of CSI-BAP were functional and viable. Phase-contrast micrograph of CSI-BAP was examined (D); dark areas stand for the existence of islets between chondrocytes sheets. The CSI-BAP was fixed with 4% paraformaldehyde solution for the histological studies (E).